---

**Article:**
Bagchi, Suman, Tayyab, Mohammad, Pasley, John Richard orcid.org/0000-0001-5832-8285 et al. (3 more authors) (2021) Quasi mono-energetic heavy ion acceleration from layered targets. Physics of Plasmas. 023108. ISSN 1089-7674

https://doi.org/10.1063/5.0022622

---

# Quasi Mono-Energetic Heavy Ion Acceleration from Layered Targets

Suman Bagchi,[1,*] Mohammad Tayyab,[1,2] John Pasley,[3]
A. P. L. Robinson,[4] Maheshwar Nayak,[5,2] and Juzer Ali Chakera[1,2]

[1] *Laser Plasma Division, Raja Ramanna Centre for Advanced Technology, Indore 452013, India*
[2] *Homi Bhabha National Institute, Training School Complex, Anushakti Nagar, Mumbai 400094, India*
[3] *York Plasma Institute, Department of Physics, University of York, York, YO10 5DD, U.K.*
[4] *Central Laser Facility, STFC Rutherford Appleton Laboratory, Harwell Campus, Didcot, OX11 0QX, U.K.*
[5] *Synchrotrons Utilization Section, Raja Ramanna Centre for Advanced Technology, Indore 452013, India*

In the present work we demonstrate acceleration of quasi monoenergetic heavy ions during the interaction of a high-intensity short-pulse laser with multi-layer targets. The targets, consisting of layers of High-Z (Gold) and low-Z (carbon) species a few nm thick, have been used to tailor the energy spectra of the high-Z ion species. Au-ion bunches of energy around 500 keV with an energy spread of less than 20% are observed. PIC simulations provide explanation for a number of features of the experimental observations. Several behaviours, in addition to the expected sheath-field acceleration, were found to be involved. It is found that the Au layer is pistoned outward by the underlying Si substrate whilst simultaneously being tamped at its leading edge by the carbon overlay. The simulations show best agreement with the experiments when the carbon layer is first rarefied by the laser prepulse. In these cases the simulations reproduce the double-humped spectra found in the experiment. Ion-electrostatic instabilities rapidly lead to the formation of a single trapping-like structure in phase space of relatively long wavelength. This long-lived structure dominates the ion acceleration and produces a double-peaked energy spectrum. It is suggested that the instability responsible may be of the Pierce-type.

## I. INTRODUCTION

The field of ion acceleration driven by intense laser pulses is continuously growing with its primary aim being compact, cost effective and high quality ion sources. With an increasing number of high power PetaWatt class laser installations around the globe [1], new results pertaining to recently explored regimes of ion acceleration are regularly presented in the literature, addressing various aspects of the acceleration process. Laser-driven MeV-scale ion acceleration came to prominence following the advent of CPA lasers and laser-plasma interactions above 10 TW [2–6]. Such ions have been suggested for use as an igniter beam in fast ignition schemes for inertial confinement fusion [7]. Whilst early experiments were based around large Nd-glass CPA lasers with pulse durations of around 1 ps, more recently the advent of high intensity Ti-Sapphire lasers with pulse durations on the order of tens of femtoseconds has demonstrated that bright ion beams can be produced with high repetition rate lasers that are more suited to practical applications [8].

However, there are still several challenges that need to be addressed. These include the achievement of precise control of the ion energy, flux and accelerated species, shot-to-shot reproducibility, and increasing both the average flux and the laser-to-ion conversion efficiency. Many laser-driven ion acceleration mechanisms have been proposed and investigated both theoretically and experimentally[9]. One of the most widely studied mechanisms is Target Normal Sheath Acceleration (TNSA) wherein ions are accelerated by the sheath field setup by hot electrons as they leave thin foil targets [10]. TNSA is a relatively simple, robust, easily implemented scheme with good repeatability. However, the ions accelerated through TNSA normally exhibit broad energy distributions and the technique favours the acceleration of lighter species such as hydrogen and carbon ions which are normally present as surface contaminants. In addition to TNSA there are a few advanced acceleration mechanisms which include Radiation Pressure Acceleration (RPA) [11], Collisionless Shock Acceleration (CSA)[12] and the Breakout Afterburner (BOA) [13]. These mechanisms offer the possibility of accelerating ions to high energies with quasi-monoenergetic features. Other schemes rely upon specific target geometries or micro-/nano-structuring, in order to modify the ion-beam production [14–16, 22]. Although there are several successful proof-of-principle experimental demonstrations of these advanced acceleration schemes, the repeatability and consistency of these schemes are still being established. This is mainly due to the fact that these mechanisms demand stringent conditions on laser and target parameters which are quite challenging to achieve on a routine basis. Another important point to be noted here is that majority of the reported studies are mainly focussed on lighter ions and, in comparison, studies of heavy-ion acceleration are rare. It is important to note here that recent experimental reports [18, 19] suggest heavy ion acceleration using high-contrast, ultra-high intensity laser pulses with ultra-thin (10 - 250 nm) metal foils. These results are explained on the basis of coulombic interactions during the expansion phase. Another set of experiments involves onset of relativistic induced transparency [20, 21] of the thin (100 nm to 250 nm) foil

* Corresponding author:sbagchi@rrcat.gov.in

target under consideration and results is narrow energy spread of lighter ions with high peak energy for specific charged states. On the contrary, our aim here is to generate quasi-mono-energetic heavy ion beam.

The difficulty in experimentally diagnosing the detailed dynamics of microscale targets driven with fs or ps pulses has led to extensive investigation of the topic via computer simulation [11, 23–26]. Such studies, typically based around the use of particle-in-cell (PIC) techniques, are however often quite limited in the range of physics that can be captured, and also in the spatio-temporal scale of the problem that can be successfully tackled, given finite computational resources. Such simulations, supported by experimental investigations, have however enabled many aspects of the physics of laser-driven ion production to be clarified, and have revealed the importance of a variety of underlying mechanisms such as Weibel instabilities, and the role of laser prepulse in such interactions [27–31].

In addition to the aforementioned acceleration schemes, there have been several theoretical and experimental reports on multi-species plasma expansion predicting quasi-monoenergetic features (energy bunching) in the ion energy spectrum. Modulations in proton energy spectra in an expanding plasma comprising two ion species (carbon ions and protons) have been observed [32–34]. Specifically it has been shown that in a two-species plasma consisting of heavy and light ions, the expansion dynamics can act to narrow the energy spread of the lighter species. The dynamics of the accelerating electric field structure is governed by the heavy ion species and the lighter particles behave like test particles. It has been concluded that only targets containing lighter species in the minority will result in a quasi-monoenergetic peak in the energy spectrum of the lighter species. Although there are several analytical and simulation studies which clearly predict spectral peaks in the lighter species energy distribution from such targets, the extent to which this mechanism has been demonstrated experimentally is somewhat limited. One clear experimental demonstration in a spherical geometry is given in reference [35]. In contrast to the previous work on multi-species plasma expansion, here we present spectral narrowing or energy bunching in heavier ion species in a target where the heavy ion species are in the minority. Quasi-monoenergetic Au-ion bunches with all the charge states having similar energies were observed from layered targets of Au and carbon deposited on a Si substrate. Interesting signatures of charge-exchange recombination in multi-species expanding plasma were observed. Numerical modelling and PIC simulations help to explain the basic features of the experimental observations.

The current work is motivated by our earlier experimental work on Au ion bunching from nano-composite targets where Au nano-particles of 3-8 nm size with a total concentration of 2- 4% by atomic weight, were randomly distributed in a 120 nm thick carbon layer deposited on either an Aluminium or a Silicon substrate [36]. Quasi-monoenergetic Au-ion bunches with energies in the few 100 keV range and having an energy spread of less than 10% were observed with all the charge states having the same energy. Experimentally it was established that the Au ions were accelerated by the thermal pressure of the expanding hot plasma instead of by the hot electron induced charge sheath separation field. The heavy Au ions, being pushed by the expanding hot plasma and restrained by the low-Z background plasma, ultimately ended up with a reduced energy spread. The presence of a low-Z carbon matrix was found to be essential for achieving a quasi-monoenergetic heavy ion beam. Simply employing an Au layer inevitably yielded Au ions with a broad energy distribution. The primary motivation behind the present experiment was to verify our earlier hypothesis regarding quasi-monoenergetic Au-ion expansion. However, in the current, more elaborate, experiment, some new and interesting physics is observed. In the present experiment, in order to try and clearly establish the role of the different ion species in the acceleration mechanism, layered targets of Au and carbon have been employed in place of the Au -carbon nanocomposite (AuNP-C) targets used previously.

## II. EXPERIMENTAL DETAILS

A schematic of the experimental set-up is shown in Fig. 1 (a). The experiment was performed using a 25 fs, 150 TW, Ti: Sapphire laser system. For the present experiment the available laser energy was around 1 Joule (40 TW). The laser is focused onto the target using an f/3 off-axis parabolic mirror at a 45° angle of incidence, with a resultant peak intensity of $1.5 \times 10^{19} W/cm^2$. The interaction chamber has been kept at a vacuum pressure of $5 \times 10^{-5}$ mbar. As mentioned earlier, the targets used consist of high–Z (Au, 5nm) and low–Z (C, 10 - 40 nm) layers deposited on a Si substrate. The main difference between these layered targets and the AuNP-C nano-composite targets that were employed previously lies in the method of deposition. In AuNP-C targets, Au and carbon were co-sputtered and the Au was present as nano particles (3-8 nm size) which were randomly embedded in the 120 nm thick carbon matrix. However, in the present scenario, Au and carbon are deposited in sequence using an electron beam evaporation system operating at a base pressure of $1.8 \times 10^{-6}$ mbar. First a thin layer of Au (5nm) is deposited onto the 1 mm thick Si substrate, and then, on top of this, a carbon layer of varying thickness (10, 20 and 40 nm) is deposited. The deposition rates of the gold and carbon layers have been kept at 1.8 nm / min and 1.2 nm /min respectively. Hereafter, a target which comprises a single layer of carbon coated onto a single layer of Au on a Si substrate will be referred to as a single-layer target and will be denoted as $^*C/Au/Si$ where the asterisk indicates the front surface (i.e. that upon which the laser is initially incident). Similarly, a double-layer target implies one in which two

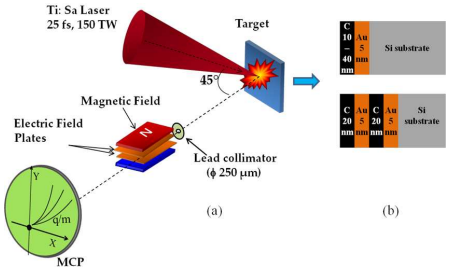


FIG. 1: (a)Schematic of the experimental set up.(b)Simple illustration of both the single- and double-layer targets.

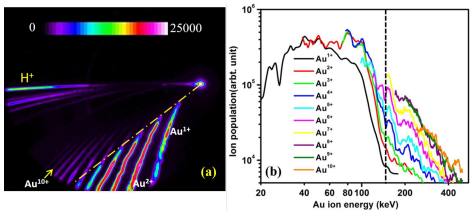


FIG. 2: (a) Typical heavy Au-ion parabolic traces recorded in TPIS using pure Au targets with no carbon coating. The yellow dashed line drawn from the origin indicates that the lower energy populations have the same maximum energy. The corresponding Au-ion energy spectra are plotted in (b).

such layers of Au and carbon have been coated onto a Si substrate i.e. $^{*}C/Au/C/Au/Si$. A simple illustration of the target configuration is shown in Fig. 1 (b).

The primary diagnostics used in the experiment to monitor ion emission characteristics was the in-house developed Thomson Parabola Ion Spectrograph (TPIS) which applies parallel electric and magnetic fields to disperse incoming ions along parabolic trajectories as per their charge-to-mass ratio. A micro-channel plate (MCP) has been used as a two-dimensional detector to record the parabolic traces of ions of different charge states simultaneously and on a single-shot basis. An Electron Multiplying-CCD (EMCCD) camera having 16-bit dynamic range (not shown in the schematic) is then employed to record the parabolic trajectories and store them for further post-processing.

## III. EXPERIMENTAL RESULTS

### A. Au-ion energy spectra from uncoated Au targets

First, we shall concentrate on the results from a pure Au coated substrate target i.e. there is no C layer at all. One typical representative TPIS image along with derived Au-ion energy spectrum is shown in Fig. 2. With only an Au layer, the Au-ions energy spectra are mainly continuous or have broad energy distributions. Another interesting point to note here is that apart from being continuous in nature most of the shots from simple Au layer targets show two distinct ion populations with different characteristics indicating that the underlying acceleration mechanisms may be different in nature.These two populations can be easily identified by noting the discontinuity in the corresponding parabolic traces (Fig. 2(a)) and also highlighted with the yellow dotted line also known as a constant velocity line drawn from the origin (neutral spot). The ion populations above and below this line have different characteristics. In Fig. 2(b), the dip in the energy spectrum which lies between these two distinct populations is indicated by the red arrow. The ion populations lying above the dashed line in Fig. 2(a) comprise mostly higher charge states and have higher energies; the maximum Au ion energy increases with charge state. This is a typical characteristic of ions accelerated by the space-charge dominated sheath-field. For the population sitting below the yellow dashed line in Fig. 2(a), which consists of low-charged states, having lower energy, but relatively higher flux, the maximum Au ion energy is similar from one charge state to the next. Therefore, it is clear that two different acceleration mechanism and/or two different sources are involved in the production of these spectra. The lower energy populations are produced by hydrodynamic expansion. Whereas the higher energy populations (for which Au ion energy increases with charge state), are produced by sheath-field acceleration. In these experiments, Au coating thicknesses of 5 nm, 10 nm and 20 nm were used, and all show similar behaviour.

### B. Carbon-gold single layer targets

As mentioned earlier, we studied the effect of introducing a carbon layer over the Au, on the Au ion acceleration. Carbon layers of varying thickness 10 nm, 20 nm and 40 nm were deposited on top of the 5 nm Au layer. All other parameters were the same as those for the uncoated Au targets. The impact of the carbon layer on the accelerated Au ion spectra are shown in Fig. 3. The parabolic traces recorded by the TPIS are also shown for more insight. It is interesting to see that even a 10 nm thick carbon layer significantly affects the Au-ion energy spectrum. With further increase of the carbon layer thickness (20 nm and 40 nm), steady reduction in the Au-ion energy spread is observed. As in the case of the uncoated Au targets; the Au-ion parabolic traces have a discontinuity, indicating the formation of two distinct

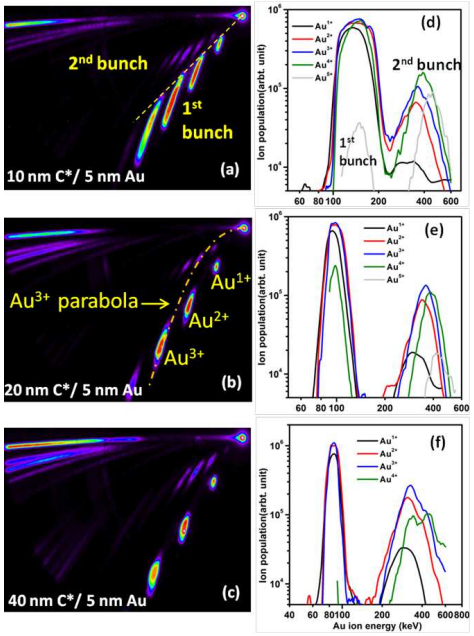


FIG. 3: Influence of the carbon layer thickness upon the Au-ion energy spectrum. (a)–(c) show typical ion signals recorded using the TPIS from targets with a single layer of carbon, over a single layer of Au deposited on Si substrate. The layer thicknesses are mentioned for each case. The Au parabolas are discrete indicating their bunched nature. A yellow dashed drawn from the origin (neutral spot) in (a) is a constant velocity line. The Au-ion energy spectrum for each case is plotted adjacent to each image (d-f).

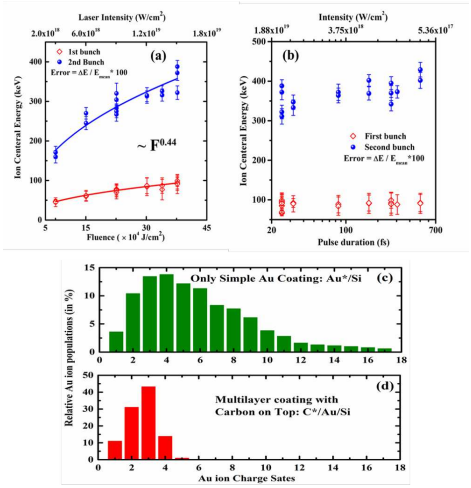


FIG. 4: Effect of laser fluence (a) and pulse duration (b) on Au ion bunching from single layer 40nm C*/5nm Au/Si target. The upper horizontal axis represents the change in laser intensity. The error bars (amplified by 100x)show the relative energy spread of the bunches with respect their mean energies. Relative abundance (in %) of gold ion charged states for the samples (c) without carbon coating layer and (d) with carbon coating layer.

populations as shown in Fig. 3(a). To elaborate further, a representative an Au-ion parabola for $Au^{3+}$ has been drawn in Fig. 3(b) to show that these bunch-like features belong to different parabolic traces and therefore correspond to different charge states.

Therefore, here again there are two distinct Au ion population albeit with reduced energy spread. As shown in Fig. 3(a), the part of the Au ion population below the yellow dashed line (constant velocity line) will be referred to as the first bunch and those above the line will be referred to as the second bunch. The impact of the carbon layer thickness on the quasi-monoenergetic production of Au ions in different shots is summarized in Fig. 4. It is clear from Figures (3) and (5) that with increase in carbon layer thickness, Au-ion energy spread reduces. The first bunch appears to be more sensitive to the carbon layer thickness while the second bunch is relatively less sensitive. With increase in carbon coating layer thickness, the energy spread of the first bunch appears to reducing and the overall spread in ion energy distribution to contained within 10 - 30 %. In comparison with recent reports in the literature [17, 20, 21], we find this behavior quite comparable keeping in mind that the scenarios are entirely different in our case. Notably, as shown in Fig. 3 (d-f), in first bunch all the Au charge states have an almost identical energy distribution whereas in the second bunch, the Au-ion energy distribution shifts slightly toward higher energy with increased charge state. Here it also important to note that for the $^*C/Au/Si$ targets the recorded Au ionization states are limited to $5^+$ whereas for the Au/Si targets (i.e. the uncoated Au targets) the observed ionization states were typically above $15^+$.

Therefore, a simple comparison between the carbon coated and uncoated targets shows a fair degree of similarity, except that in the former case the Au ion energies, as well as the observed charge states, are reduced. However the proton and carbon ion spectral characteristics remain unchanged and both exhibit continuity in the energy distribution. The scaling of gold ion energies with laser pulse fluence as shown in figure 4 (a and b) also point towards a new acceleration mechanism. As

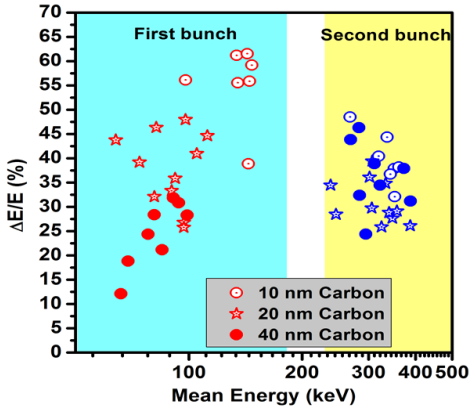


FIG. 5: Observed Au-ion energy spread in the first and second bunches with respect to different carbon layer thicknesses in $^*C/Au/Si$ targets. Each data point represents an individual shot onto a pristine sample.

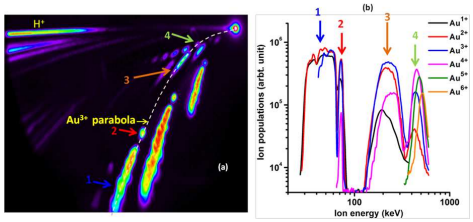


FIG. 6: (a) Au-ion spectra recorded from double-layer targets show two pairs of energy bunches. A parabolic trace for $Au^{3+}$ is drawn to show that the bunched structures are part of different Au-ion parabola, corresponding to different ion states. The energy spectra for different Au-ion charge states are plotted in (b). The Au-ion bunch at around 500 keV, indicated by number 4, has an energy spread of less than 20%.

discussed earlier, for the known ion acceleration mechanisms, the maximum ion energy scales with the laser pulse intensity rather than its fluence. On the contrary, we observe here that the gold ion energy scales as $F^{0.44}$ with laser pulse fluence, a strong indication of pressure induced hydrodynamics expansion behavior. Moreover, the insensitivity of gold ion energies with increasing laser pulse duration indicates that the underlying mechanism has to be non-Coulombic in nature. This makes the demonstrated scheme not limited to ultra-short pulsed lasers only.

### C. Results from double layer targets

The shots onto double-layer targets ($^*C/Au/C/Au/Si$) also clearly exhibit energy bunching. Similarly to single-layer targets, double-layer targets also showed two sets of discrete bunches in many shots. One such representative shot is shown in Fig. 6 (a). The corresponding Au-ion energy spectrum is plotted in Fig. 6(b). To clarify, each dot like feature in Fig. 6(a) is actually part of a different Au-ion parabolic trace. A parabolic trace for $Au^{3+}$ has been overlaid onto the TPIS image. Also each part of the $Au^{3+}$-ion population is marked with different colour arrows and numbers to allow us to refer to them more clearly (Fig. 6b). A similar numbering scheme is applied to other charge states as well. It is interesting to see that each charge state of Au shows similar characteristics. From this study, when considered alongside the single-layer results, it becomes clear that the Au layers immersed at different depths in the carbon matrix are producing bunches of clearly distinguishable energy. In the shot shown in Fig 6, the Au-ion bunches at 0.5 MeV have an energy spread $\Delta E/E$ of less than 20%. We thereby demonstrate that such multi-layer targets can be effectively used for accelerating heavy ions with quasi-monoenergetic features.

## IV. MODELLING AND DISCUSSION

First let us compare these results with the results obtained with the Au-carbon nano-composite target used in the previous experiment. The present experiments clearly establish the role of the low-Z carbon layer in obtaining quasi-monoenergetic Au ions. However here, in addition, some interesting new features are also observed. With the introduction of the carbon layer, two distinct bunches of quasi-monoenergetic Au ions appear, unlike in the case of the pure Au targets which mainly show a broad energy distribution. Although there is some shot-to-shot variation in the energy of the observed bunches, overall it is clear that they belong to one of the two distinct energy-bunches. This is in contrast to the previous experimental campaign with AuNP-C nanocomposite targets. In that case most of the shots showed a single energy bunch of Au ions (80% of total number of shots taken) while two or multiple bunches were observed in the remaining 20% of cases. However, in the present case, with layered targets, the formation of two bunches occurs in most shots. In addition the two bunches seem to be accelerated by two different mechanisms (all the charge states in the first bunch have exactly the same energy whereas in the second bunch; the energy slightly increases with charge state).

Now let's come to the energy characteristics of the two bunches. As mentioned earlier, a close inspection of the observed ion traces in the TPIS and the energy spectra

from Au/Si and $^*C/Au/Si$ targets shows a strong correlation. In other words, the observation of two bunches from the $^*C/Au/Si$ layered target seems to be linked with the observation of two different populations in the uncoated Au targets presented earlier.

To further elucidate the physical mechanism that underpins the observations made using these targets, a number of one-dimensional (1-D) Particle-in-Cell (PIC) simulations are carried out. Of the different targets presented in this paper we have concentrated on the C-Au-Si (single carbon layer) target only. In the first instance we consider an ideal initial condition for the target following laser irradiation, in which the target has a step-like density profile and is heated to a uniform electron temperature. We ignore any 'fast' component to the electron distribution. This problem is simulated using the 1-D collisionless electromagnetic PIC code, ELPS. Our baseline model (Run BL) for this configuration consists of a carbon substrate with a density of $1\times10^{29}m^{-3}$ (fully ionized), a 5 nm Au layer ($Z^* = 40$), and a 20 nm carbon layer (again fully ionized). Here we use $Z^*$ to denote the effective charge of the Au ions. All Au ions are assigned this effective charge in these fixed ionization simulations. The ion density for the Au layer is set at $5 \times 10^{28}m^{-3}$ (85% of solid density). The grid consists of 250,000 cells with a cell width of 0.2 nm (i.e. 50 micron length in total). The front of the substrate is set at x = 25 $\mu$m. The plasma is initially neutral, with the electrons having a single-temperature Maxwellian distribution ($T_e = 2$ keV). This simulation is run up to 380 fs. The choice of $Z^*$ and initial temperature was informed by the following considerations : (i) the experimentally observed ion energies ($\epsilon_{ion} \propto Z^*k_BT_e$), (ii) observation of high temperatures in thin surface layers in other experiments [42], and (iii) predictions of the Thomas-Fermi model regarding the expected charge states under these conditions. Note that it has been assumed that the short pulse duration and thick substrate imply a limited contribution from the fast electrons. Instead, it is conjectured that strongly heated ($T_e$ = 2keV) background electrons drive the ion acceleration. The resultant energy spectrum of the gold ions is shown in Fig. 7. We can see that the energy spectrum is clearly peaked at relatively high energy (around 350 keV), so even in this baseline simulation we find that we produce a strong 'narrow-band' feature in the energy spectrum albeit with a large dark current. To be clear: in this simulation (and the others that are reported on) the principal mechanism that is accelerating the ions is plasma expansion, or TNSA. However the energy spectrum experiences strong modifications due to effects associated with the multi-species / multi-component nature of the target. One argument for why we might expect a narrow-band spectrum is based on the established understanding of plasma expansion: the gold forms a relatively thin inhomogeneity in the plasma expansion, and is behind the initial plasma-vacuum interface. If the gold ions were just a relatively light dopant, and behaved as tracer particles, then they would experience a region where the electric field has high spatial uniformity. Thus, in the limit where the gold layer is thin, we expect the energy spectrum to be relatively narrow. In this simulation none of these conditions hold particularly well, however the spectrum is still strongly peaked because of the pistoning effect of the substrate ions and the tamping effect of the ions in the carbon layer. Because these two layers so strongly influence how the gold ions evolve, the details of the spectrum can be quite sensitive to the exact initial conditions. Although this baseline simulation shows one strong narrow-band feature, it does not show the two narrow-band features that were found in the experiment. To explore further, we focus on the two possibilities: a) that it relates to the details of the initial conditions, or b) that it relates to (micro) physics not included in the baseline simulation.

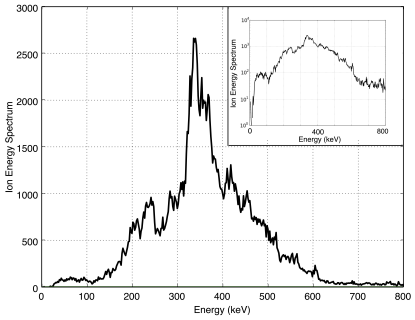


FIG. 7: Au-ion spectrum from the baseline (Run BL) 1D PIC simulation at 380 fs. The inset shows the same graph with vertical axis in logarithmic (log10) scale to reveal the large dark current associated with the peak structure.

In exploring the first possibility, we find that if the outermost C layer is pre-expanded (i.e. of greater extent and lower density), which could occur due to the effects of laser pre-pulse, then when the density was between 1 % and 10% of solid density (and increased to 200 $\mu$m thickness, with $Z^* = 30$ for the Au ions) that a double-peaked spectrum results (other aspects of the simulation remain fixed with respect to the baseline conditions). This deformation of the initial target profile is consistent with the range of expected pre-pulse, based on 1D radiation-hydrodynamics simulations performed using the HYADES code [43]. The results of a simulation with a C layer at 5% of solid density (Run A1) are shown in Fig. 8(a) and those for a simulation with a C layer at 2.5% of solid density (Run A2) are shown in Fig. 8(b). In all of these simulations we notice that the effect of ion-electrostatic instabilities is dominant [40], however for these initial conditions we find that instability

rapidly generates a single trapping-like structure in phase space with relatively long wavelength. This long-lived structure then dominates the energy spectrum and produces a double-peaked energy spectrum. This is shown in fig. (9). The trapping structure forms relatively early on (100fs), and persists for a long time (beyond 200fs), however at late time it breaks up (300fs) leaving two accumulations in phase space that form the two peaks in the energy spectrum. The instability responsible for this could be the streaming or Buneman instability If the two-stream instability is posited as the cause of this feature, then the long wavelength of this feature requires special explanation. The spatial and temporal inhomogeneity of this problem mean that the textbook formulation of the two-stream instability cannot be applied in a straightforward manner. However the wavenumber should scale as $k \propto \omega_p/u$, where $u$ is the velocity of streaming ions, and $\omega_p$ is the plasma frequency of the gold plasma. A long wavelength implies fast streaming ions. The gold layer will encounter this at early times as the fastest substrate ions stream through it. At this time we have : $\omega_p \approx 10^{14}\mathrm{s}^{-1}$, and $u \approx 10^6\mathrm{ms}^{-1}$, so $k \approx 10^8\mathrm{m}^{-1}$. This is compatible with the scale of the phase space structure, so the two-stream instability might account for this. However the isolated nature of this structure suggests that other instabilities might be responsible, such as one similar to the Pierce instability [37] (which is often associated with double layer formation and ion trapping) may be responsible [38]. So although the two-stream instability could account for this spectral modification, a precise determination of the mechanism at work requires much more extensive investigation than has been performed here, and will be the subject of future investigation.

To explore the possibility that non-inclusion of microphysics in the baseline simulation is responsible for the second narrow-band feature, we consider the possibility that recombination is responsible for such double peaked structure formation. In order to gauge the effect that this could have on the energy distribution, we include recombination alone, without any ionization processes, which should maximize the effect that this has. In principle, three-body recombination, radiative recombination, and dielectronic recombination could all contribute. Rates for these processes can be determined from the formulae provided by Djaoui and Rose [39]. By calculating rates for typical conditions, we determine that dielectronic recombination has the fastest rate by a substantial margin. We therefore incorporate dielectronic recombination alone into a modified version of the PIC code, using very standard Monte-Carlo methods that are regularly used with PIC codes [41]. A number of runs are carried out, and here we shall report on two of these. In Run B1, we use a 5 nm Au layer, with a 20nm C layer on top. In Run B2 we use a 5 nm Au layer with a 40 nm C layer on top. In all of these 'B' runs the initial ion charge is set to $Z^* = 50$, with all other parameters being the same as in the baseline (BL) run. Ion energy spectra from these runs are shown in figure 9 below.

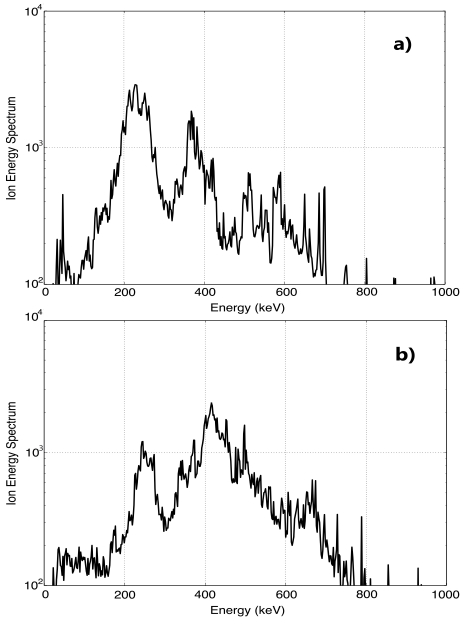


FIG. 8: Au-ion energy spectrum at 380 fs taken from simulations in which carbon layer is considered extended up to 200 nm in front of the target with densities, a) 5% of solid density (Run A1) and, b) 2.5% of solid density (Run A2) at 240 fs.

The spectra shown in figure 9 represent our general findings from looking at the effect of recombination: we still obtain a single narrow-band feature, and in some cases there is some suggestion that there could be two narrow-band features. However, what is observed in fig. 9(a) is not as clear as the effect observed in fig.8. It is also inconsistent in the sense that there are substantial differences in the strength of the effect between different charge states, and in other simulations, e.g. B2 (figure 8(b)), the effect is completely absent. We are therefore led to the conclusion that recombination is not responsible for the second narrow-band feature, and that it is unlikely that other atomic physics processes are either. The results of PIC modelling can thus be summarised as follows : (a) the principal mechanism of acceleration is plasma expansion, or TNSA, (b) however this is strongly modified by processes associated with the multi-species nature of the target, (c) one process is the pistoning effect of the substrate ions (higher charge-to-mass ratio), (d) another process appears to be a micro-instability which produces a second narrow-band feature in the energy spectrum.

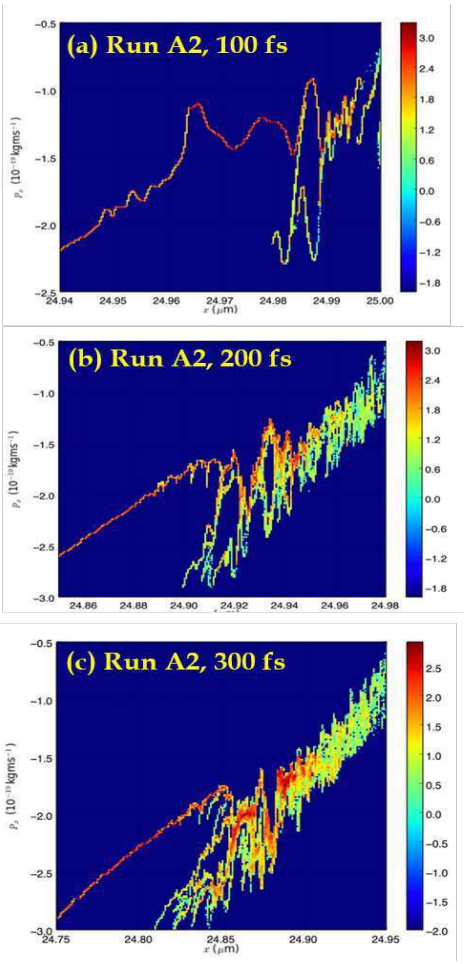


FIG. 9: Portions of Au-ion phase space at (a) 50fs, (b) 100fs, and (c) 150fs in simulation A2.

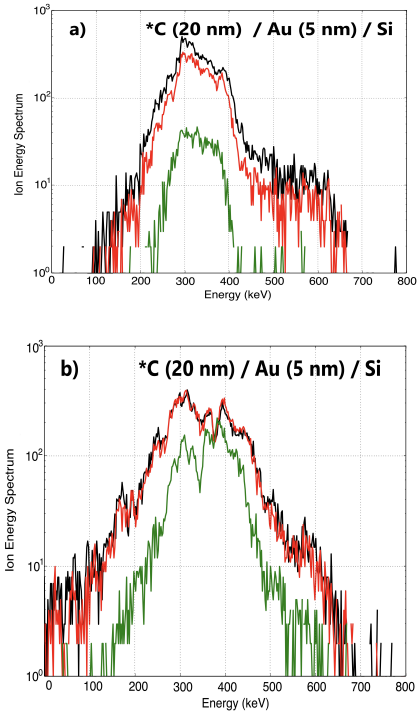


FIG. 10: Au-ion energy spectrum at 380 fs in, a) run B1, *C (20 nm) / Au (5 nm) / Si, and b) run B2: *C (20 nm) / Au (5 nm) / Si with dielectronic recombination model. Key: $Z^* = 36$ – black, $Z^* = 35$ – red, $Z^* = 34$ – green.

## V. CONCLUSIONS

Quasi mono-energetic Au-ion acceleration with different charge states of Au has been performed using multilayer targets. To the best of our knowledge, this is the first time that nano-fabricated targets have produced such striking results with a heavy ion species. It was established that the presence of a low-Z carbon layer plays an important role in producing quasi monoenergetic features in the Au-ion energy spectrum. The simulations provide some insight regarding the experimental observations. The formation of a quasi-monoenergetic feature might be expected from a thin layer expanding outward between two disparate layers, due to the uniformity of the electric field experienced by such a region. The simulations reveal a number of mechanisms at work in addition to this. The Au layer is pistoned outward by the underlying Si substrate whilst simultaneously being tamped at its leading edge by the carbon overlay. The simulations show best agreement with the experiments when the carbon layer is first rarefied by the laser prepulse. In this case the simulations reproduce the double-humped spectra found in the experiment. In these cases ion-electrostatic instabilities are abundant in the simulations, and these instabilities rapidly lead to the formation of a single trapping-like structure in phase space of relatively long wavelength. This long-lived structure rapidly

comes to dominate the ion acceleration and produces a double-peaked energy spectrum. The instability responsible for this could be the streaming or Buneman instability, however the isolated nature of this structure suggests that an instability similar to the Pierce instability may be responsible. A precise determination of the mechanism at work requires much more extensive investigation than has been performed here and will be the subject of future investigation. The effects of recombination were also investigated in detail via simulation, and found not to be significant contributing factors to the findings.

## VI. ACKNOWLEDGMENTS

The authors acknowledge the help of Ankit Singla, Sunil Meena and R. A. Khan with laser operations and S. Sebastin, K. C. Parmar and R. P. Kushwaha for mechanical support.

## VII. DATA AVAILABILITY

The data that supports the findings of this study is available from the corresponding author upon reasonable request.

[1] C. Danson, D. Hillier, N. Hopps, and D. Neely, High Power Laser Sci. Eng. **3**, e3 (2015).
[2] A. J. Mackinnon, Y. Sentoku, P. K. Patel, D. W. Price, S. Hatchett, M. H. Key, C. Andersen, R. Snavely, and R. R. Freeman, Phys. Rev. Lett. **88**(21), 215006 (2002).
[3] M. Zepf, E. L. Clark, F. N. Beg, R. J. Clarke, A. E. Dangor, A. Gopal, K. Krushelnick, P. A. Norreys, M. Tatarakis, U. Wagner, and M. S. Wei, Phys. Rev. Lett. **90**(6), 064801 (2003).
[4] R. A. Snavely, M. H. Key, S. P. Hatchett, T. E. Cowan, M. Roth, T. W. Phillips, M. A. Stoyer, E. A. Henry, T. C. Sangster, M. S. Singh, S. C. Wilks, A. MacKinnon, A. Offenberger, D. M. Pennington, K. Yasuike, A. B. Langdon, B. F. Lasinski, J. Johnson, M. D. Perry, and E. M. Campbell, Phys. Rev. Lett. **85**(14), 2945-2948 (2000).
[5] S. P. Hatchett, C. G. Brown, T. E. Cowan, E. A. Henry, J. S. Johnson, M. H. Key, J. A. Koch, A. B. Langdon, B. F. Lasinski, R. W. Lee, A. J. Mackinnon, D. M. Pennington, M. D. Perry, T. W. Phillips, M. Roth, T. C. Sangster, M. S. Singh, R. A. Snavely, M. A. Stoyer, S. C. Wilks and K. Yasuike, Phys. Plasmas **7**, 2026 (2000).
[6] E. L. Clark, K. Krushelnick, M. Zepf, F. N. Beg, M. Tatarakis, A. Machacek, M. Santala, I. Watts, P. A. Norreys, and A. E. Dangor, Phys. Rev. Lett. **85**(8), 1654-1657 (2000).
[7] M. Roth, T. E. Cowan, M. H. Key, S. P. Hatchett, C. Brown, W. Fountain, J. Johnson, D. M. Pennington, R. A. Snavely, S. C. Wilks, K. Yasuike, H. Ruhl, F. Pegoraro, S. V. Bulanov, E. M. Campbell, M. D. Perry, and H. Powell, Phys. Rev. Lett. **86**(3), 436-439 (2001).
[8] J. S. Green, A. P. Robinson, N. Booth, D. C. Carroll, R. J. Dance, R. J. Gray, D. A. MacLellan, P. McKenna, C. D. Murphy, D. Rusby, and L. Wilson, Appl. Phys. Lett. **104**(21), 214101 (2014).
[9] A. Macchi, M. Borghesi, and M. Passoni, Rev. Mod. Phys. **85**(2), 751-793 (2013).
[10] S. C. Wilks, A. B. Langdon, T. E. Cowan, M. Roth, M. Singh, S. Hatchett, M. H. Key, D. Pennington, A. MacKinnon, and R. A. Snavely, Phys. Plasmas **8**(2), 542-549 (2001).
[11] A. P. Robinson, M. Zepf, S. Kar, R. G. Evans, and C. Bellei, New J. Phys. **10**, 013021 (2008).
[12] O. Silva, M. Marti, J. R. Davies, R. A. Fonseca, C. Ren, F. S. Tsung, and W. B. Mori, Phys. Rev. Lett **92**, 015002 (2004).
[13] L. Yin, B. J. Albright, B. M. Hegelich, K. J. Bowers, K. A. Flippo, T. J. Kwan, and J. C. Fernández, Phys. Plasmas **14**(5), 056706 (2007).
[14] S. A. Gaillard, T. Kluge, K. A. Flippo, M. Bussmann, B. Gall, T. Lockard, M. Geissel, D. T. Offermann, M. Schollmeier, Y.Sentoku, and T. E. Cowan, Phys. Plasmas **18**(5), 056710 (2011).
[15] D. Margarone, O. Klimo, I. J. Kim, J. Prokůpek, J. Limpouch, T. M. Jeong, T. Mocek, J. Pkal, H. T. Kim, J. Proka, K. H. Nam, L. Tolcová, I. W. Choi, S. K. Lee, J. H. Sung, T. J. Yu, and G. Korn, Phys. Rev. Lett. **109**(23), 234801 (2012).
[16] K. Flippo, T. Bartal, F. Beg, S. Chawla, J. Cobble, S. Gaillard, D. Hey, A. MacKinnon, A. MacPhee, P. Nilson, D. Offermann, S. L. Pape, and M. J. J. Schmitt, Phys. Conf. Ser. **244**(2), 6-10 (2010).
[17] D. Haberberger, S. Tochitsky, F. Fiuza, C. Gong, R. A. Fonseca, L. O. Silva, W.B. Mori, and C. Joshi, Nat. Phys. **8**, 95 (2012)
[18] J. Braenzel, A. A. Andreev,K. Platonov, M. Klingsporn, L. Ehrentraut and M. Schnürer Phys. Rev. Lett. **114**(12), 124801-5 (2015).
[19] J. Li, P. Forestier-Colleoni, M. Bailly-Grandvaux,C. McGuffey, A.V. Areev, S. S. Bulanov, J. Peebles, C. Krauland, A. E. Hussein, T. Batson, J.C. Fernandez, S. Palaniyappan, R. P. Johnson, G. M. Petrov and F.N. Beg New J. Phys **21** 103005 (2019)
[20] Sasi Palaniyappan, B. Manuel Hegelich, Hui-Chun Wu, Daniel Jung, Donald C. Gautier, Lin Yin, Brian J. Albright, Randall P. Johnson, Tsutomu Shimada, Samuel Letzring, Dustin T. Offermann, Jun Ren, Chengkun Huang, Rainer Hörlein, Brendan Dromey, Juan C. Fernandez and Rahul C. Shah, Nat. Phys. **8**,763-769 (2012)
[21] S. Palaniyappan, C. Huang, D. C. Gautier, C. E. Hamilton, M. A. Santiago, C.Kreuzer, A. B. Sefkow, R. C. Shah, and J. C. Fernandez, Nat. Commun. **6**, 10170 (2015).
[22] A. Zigler., S. Eisenman, M. Botton, E. Nahum, E. Schleifer, A. Baspaly, I. Pomerantz, F. Abicht, J. Branzel, G. Priebe, S. Steinke, A. Andreev, M. Schnuerer, W. Sandner, D. Gordon, P. Sprangle, and K. W. Ledingham, Phys. Rev. Lett. **110**(21), 215004 (2013).
[23] T. Z. Esirkepov, Y. Sentoku, K. Mima, K. Nishihara, F. Califano, F. Pegoraro, N. M. Naumova, S. V. Bulanov, Y. Ueshima, T. V. Liseikina, V. A. Vshivkov, and Y. Kato,

JETP Lett. **70**(2), 82-89 (1999).
[24] T. Kluge, S. A. Gaillard, K. A. Flippo, T. Burris-Mog, W. Enghardt, B. Gall, M. Geissel, A. Helm, S. D. Kraft, T. Lockard, J. Metzkes, D. T. Offermann, M. Schollmeier, U. Schramm, K. Zeil, M. Bussmann, and T. E. Cowan, New J. Phys. **14**, 023038 (2012).
[25] E. D'Humìres, E. Lefebvre, L. Gremillet, and V. Malka, Phys. Plasmas **12**, 062704 (2005).
[26] Y. Sentoku, T. E. Cowan, A. Kemp, and H. Ruhl, Phys. Plasmas **10**(5), 2009-2015 (2003).
[27] S. Göde, C. Rödel, K. Zeil, R. Mishra, M. Gauthier, F. E. Brack, T. Kluge, M. J. Macdonald, J. Metzkes, L. Obst, M. Rehwald, C. Ruyer, H. P. Schlenvoigt, W. Schumaker, P. Sommer, T.E. Cowan, U. Schramm, S. Glenzer, and F. Fiuza, Phys. Rev. Lett. **118**(19), 1-5 (2017).
[28] P. McKenna, D. C. Carroll, O. Lundh, F. Nrünberg, K. Markey, S. Bandyopadhyay, D. Batani, R. G. Evans, R. Jafer, S. Kar, D. Neely, D. Pepler, M. N. Quinn, R. Redaelli, M. Roth, C. G. Wahlström, X. H. Yuan, and M. Zepf, Laser Part. Beams **26**(4), 591-596 (2008).
[29] L. Romagnani, J. Fuchs, M. Borghesi, P. Antici, P. Audebert, F. Ceccherini, T. Cowan, T. Grismayer, S. Kar, A. MacChi, P. Mora, G. Pretzler, A. Schiavi, T. Toncian, and O. Willi, Phys. Rev. Lett. **95**(19), 195001 (2005).
[30] M. Kaluza, J. Schreiber, M.I. Santala, G. D. Tsakiris, K. Eidmann, J. Meyer-Ter-Vehn, and K. J. Witte, Phys. Rev. Lett. **93**(4), 045003 (2004).
[31] P. Mckenna, K. W. D. Ledingham, J. M. Yang, L. Robson, T. Mccanny, S. Shimizu, R. J. Clarke, D. Neely, K. Spohr, R. Chapman, R. P. Singhal, K. Krushelnick, M. S. Wei, and P. A. Norreys, Phys. Rev. E. **70**(3) 036405 (2004).
[32] R. Decoste and B. H. Ripin, Phys. Rev. Lett. **40**(1), 34-37 (1978).
[33] M. Alien, Y. Sentoku, P. Audebert, A. Blazevic, T. Cowan, J. Fuchs, J. C. Gauthier, M. Geissel, M. Hegelich, S. Karsch, E. Morse, P. K. Patel, and M. Roth, Phys. Plasmas **10**(8), 3283-3289 (2003).
[34] A. V. Gurevich and A. P. Meshcherkin. Sov. Phys. JETP **53**, 5 (1981).
[35] S. Ter-Avetisyan, M. Schnürer, P. V. Nickles, M. Kalashnikov, E. Risse, T. Sokollik, W. Sandner, A, Andreev, and V. Tikhonchuk, Phys. Rev Lett **96**(14), 145006 (2006).
[36] M. Tayyab, S. Bagchi, J. A. Chakera, D. K. Avasthi, R. Ramis, A. Upadhyay, B. Ramakrishna, T. Mandal, P. A. and Naik, Phys. Plasmas **25**(12), 123102 (2018).
[37] S. Iizuka, K. Saeki, N. Sato, and Y. Hatta, Phys. Rev. Lett. **43**(19), 1404-1407 (1979).
[38] S. Eliezer and A. Ludmirsky, Laser Part. Beams **1**(3), 251-269 (1983).
[39] A. Djaoui and S. J. J. Rose, Phys. B At. Mol. Opt. Phys. **25**(11), 2745-2762 (1992).
[40] T.J.M.Boyd and J.J.Sanderson, *The Physics of Plasmas*, Cambridge University Press (2003)
[41] R.Duclous, J.G.Kirk, and A.R.Bell, *Plasma Phys. Control. Fusion*, **53**, 015009 (2010)
[42] K. U. Akli, S. B. Hansen, A. J. Kemp, R. R. Freeman, F. N. Beg, D. C. Clark, S. D. Chen, D. Hey, S. P. Hatchett, K. Highbarger, E. Giraldez, J. S. Green, G. Gregori, K. L. Lancaster, T. Ma, A. J. MacKinnon, P. Norreys, N. Patel, J. Pasley, C. Shearer, R. B. Stephens, C. Stoeckl, M. Storm, W. Theobald, L. D. Van Woerkom, R. Weber, and M. H. Key, Phys.Rev.Lett, **100**, 165002 (2008)
[43] J. T. Larsen and S. M. Lane *J. Quant. Radiat. Transfer* **51**, 179 - 186 (1994)

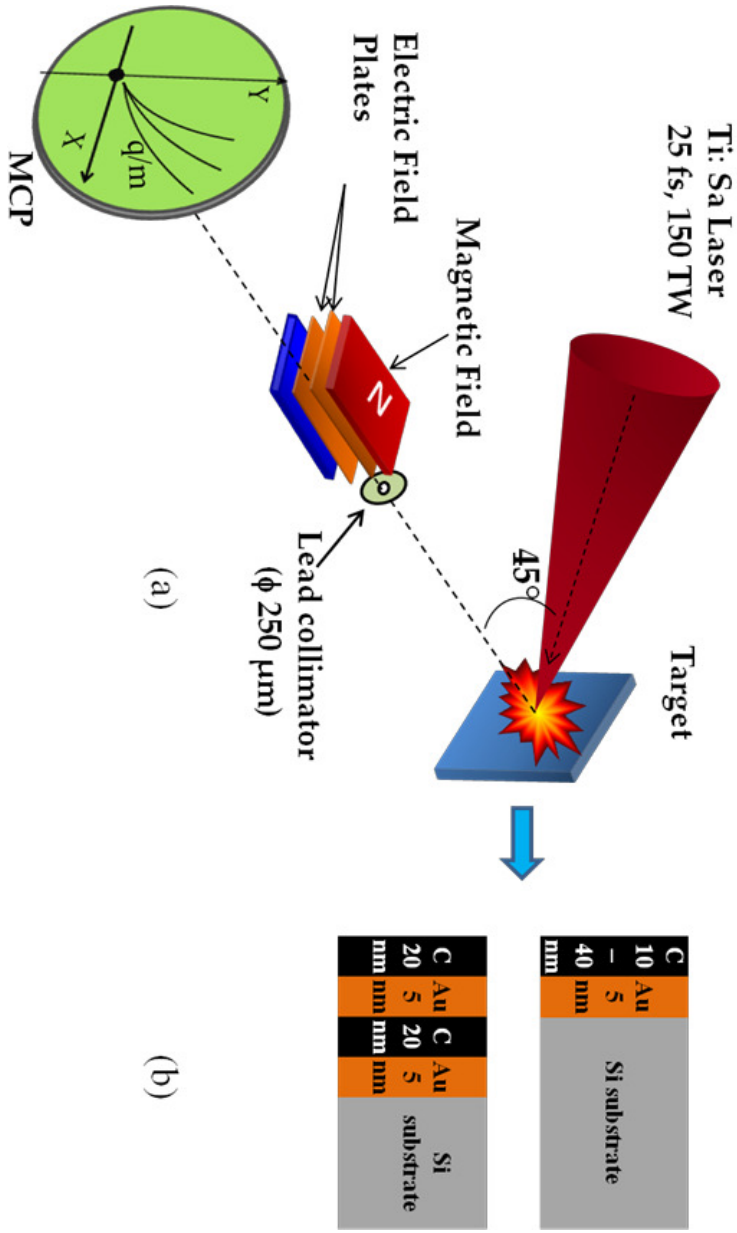

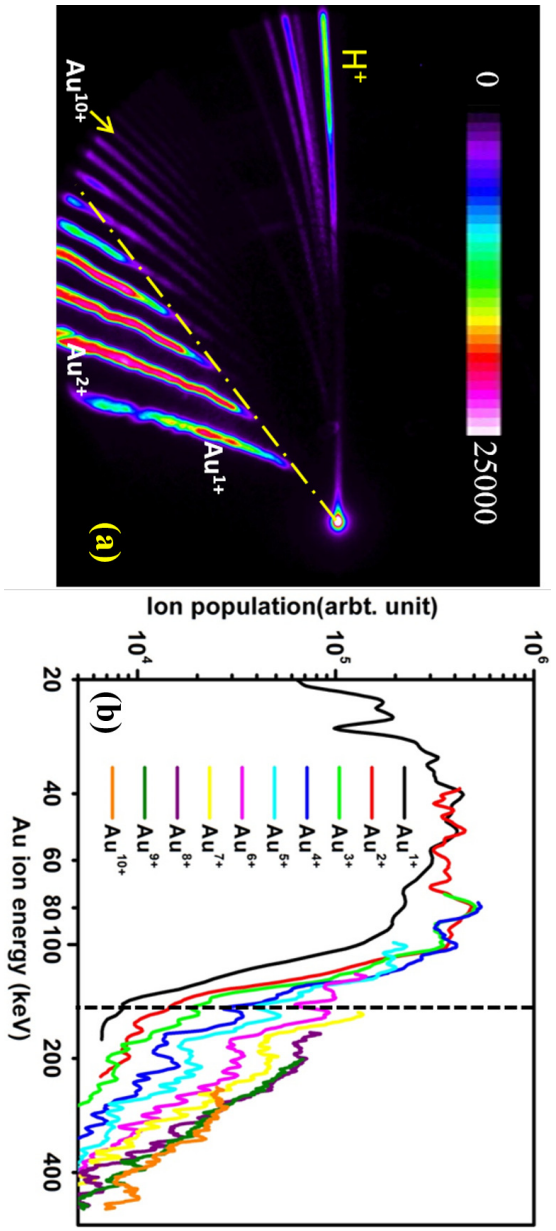

AIP Publishing

Physics of Plasmas

ACCEPTED MANUSCRIPT



PLEASE CITE THIS ARTICLE AS DOI: 10.1063/5.0022622

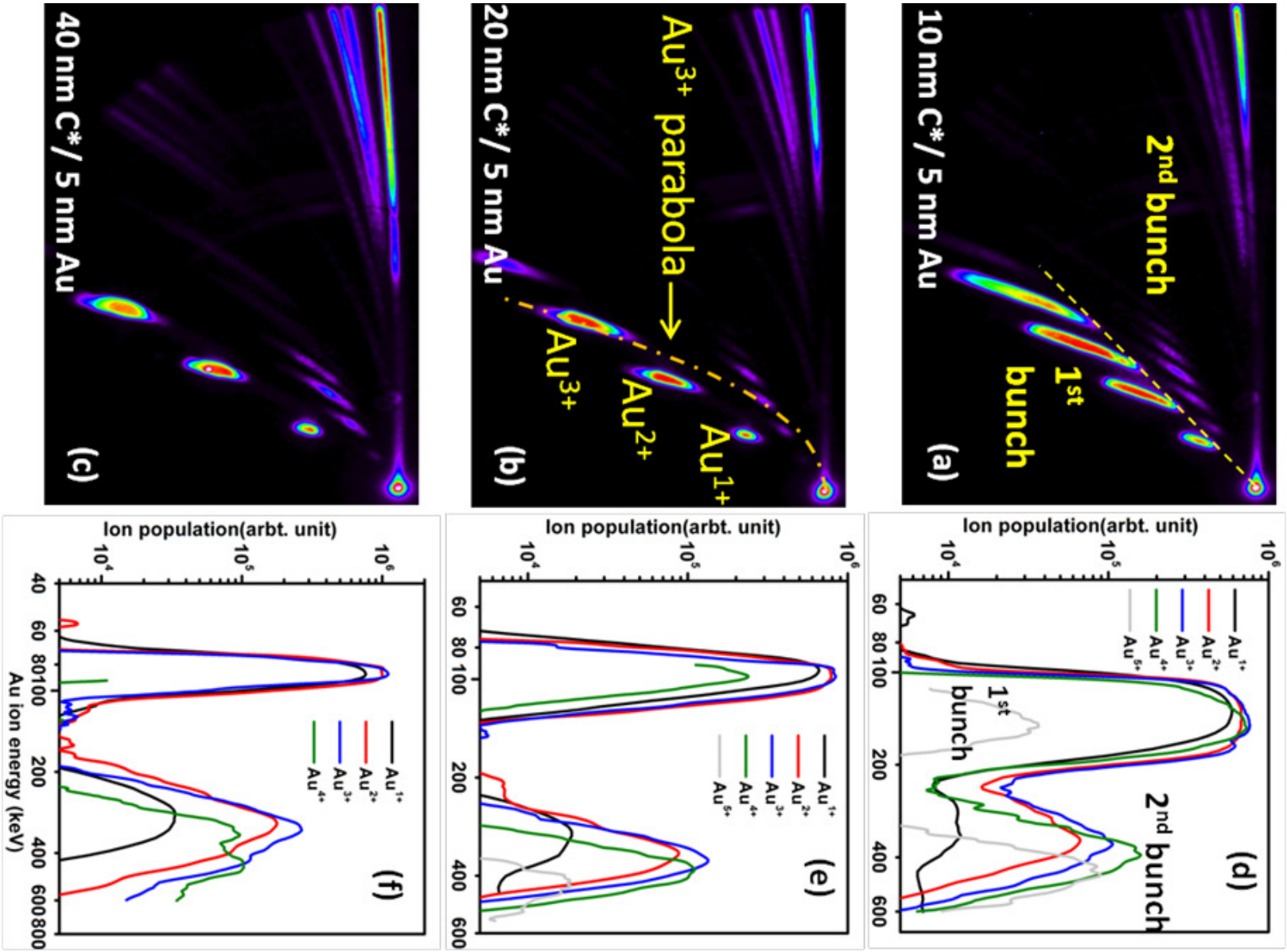

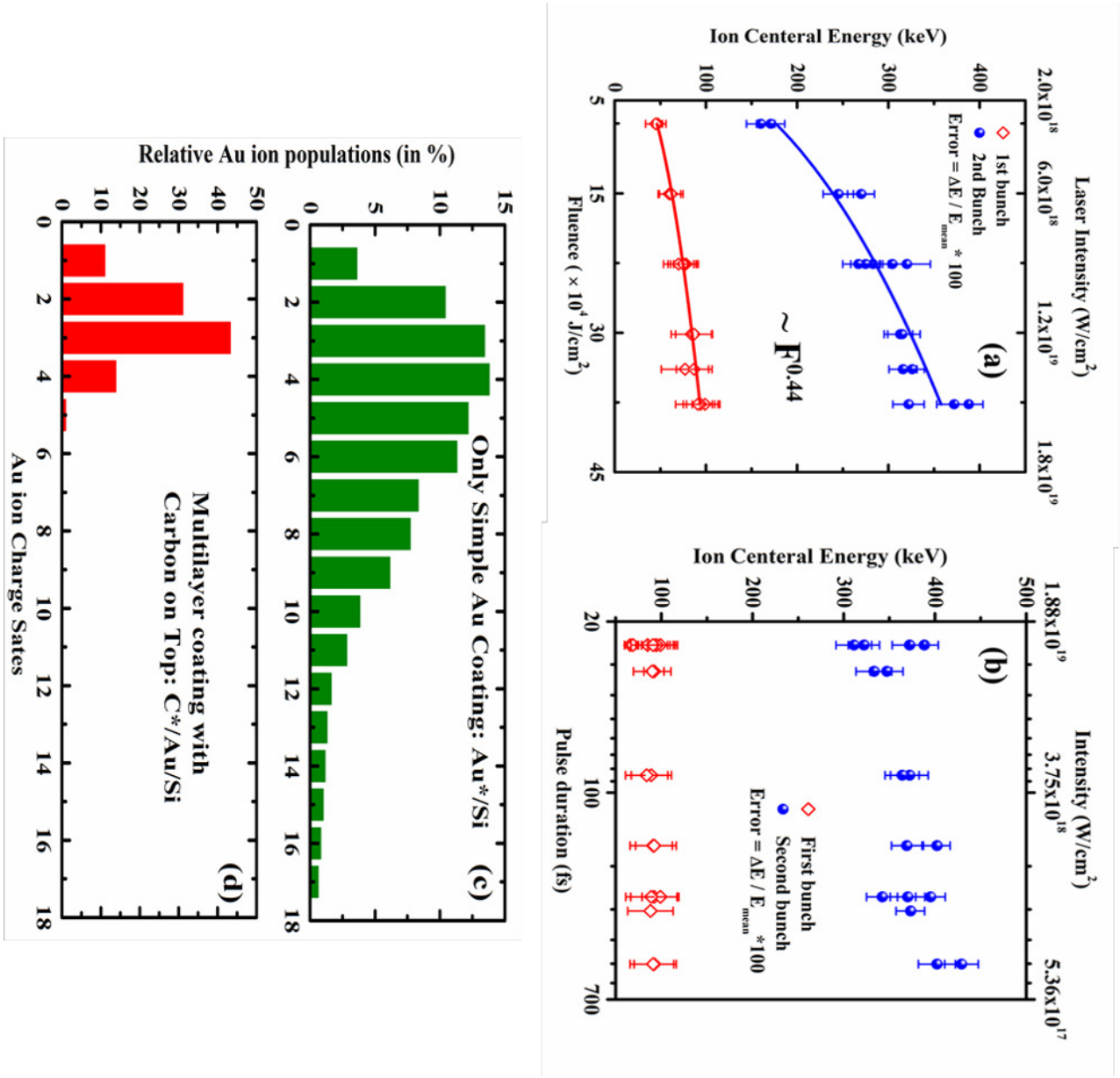

PLEASE CITE THIS ARTICLE AS DOI: 10.1063/5.0022622

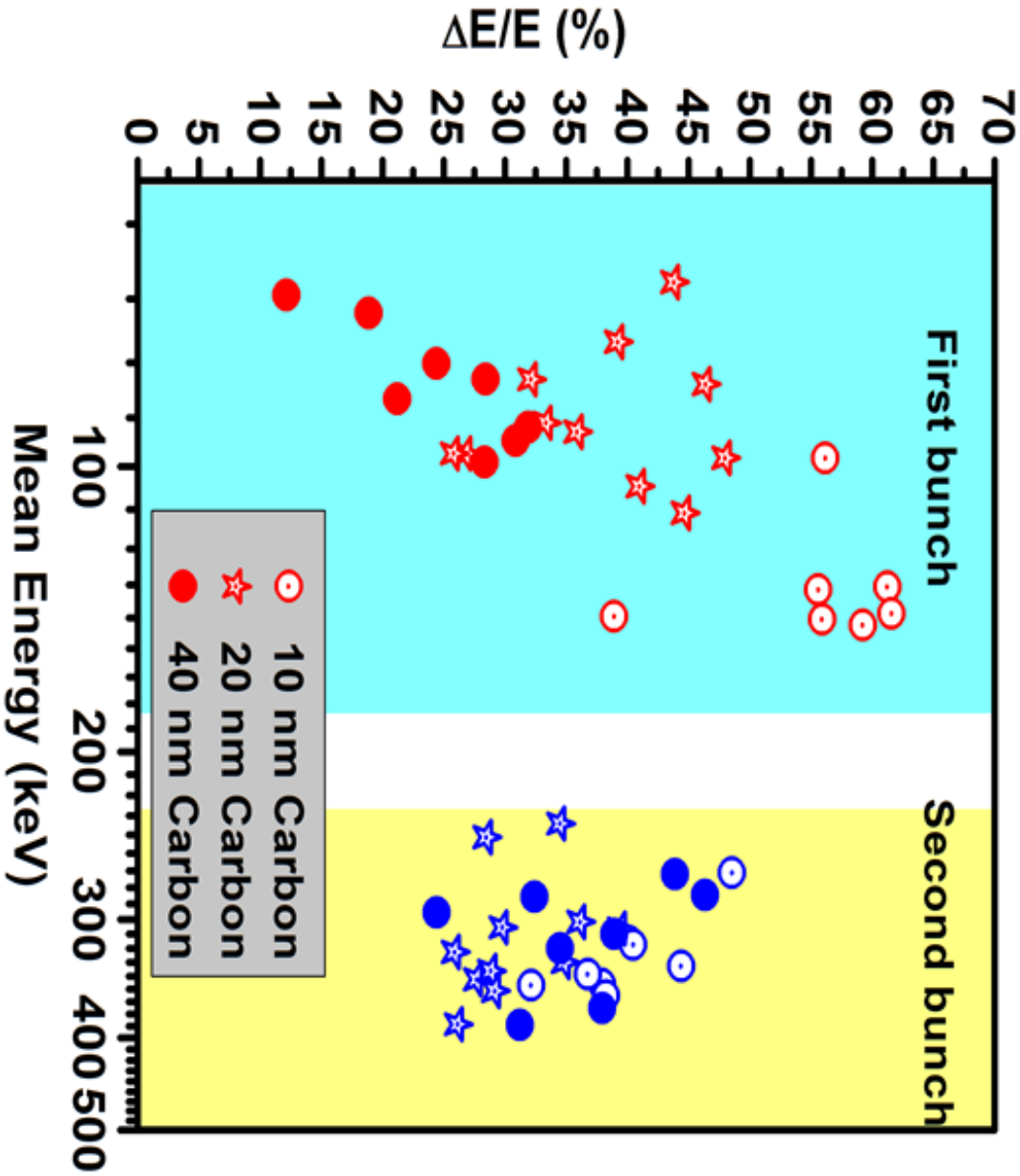

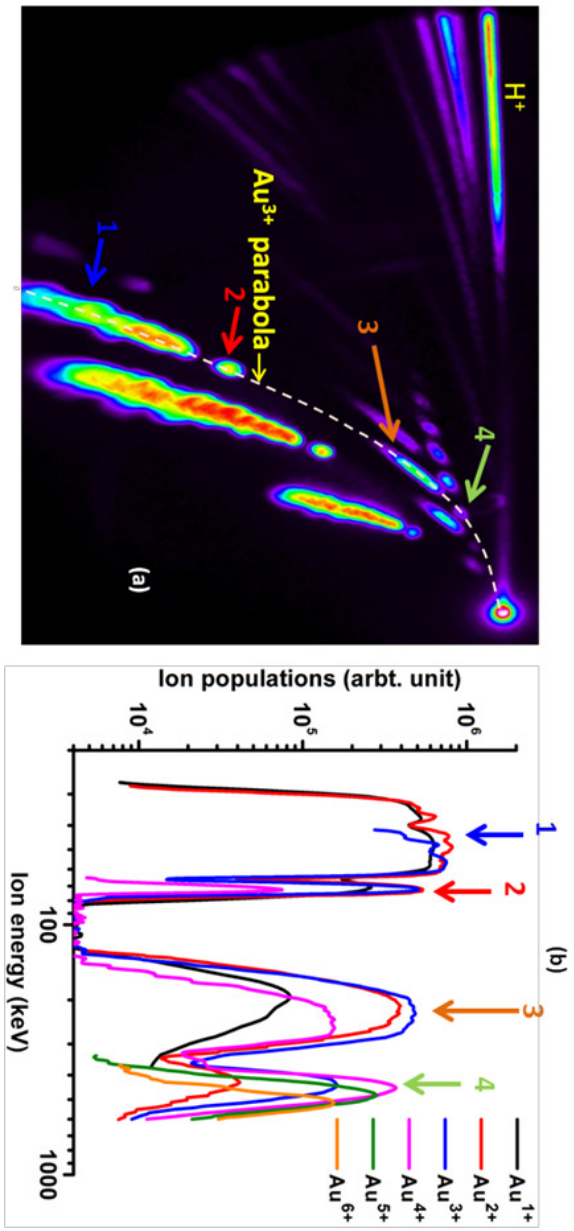

PLEASE CITE THIS ARTICLE AS DOI: 10.1063/5.0022622